Research Paper

The Bidirectional Regulation between MYL5 and HIF-1α Promotes Cervical Carcinoma Metastasis

Lan Zhang[1]*, Shu-Ting Huang[1]*, Yan-Ling Feng[1], Ting Wan[1], Hai-Feng Gu[1], Jing Xu[1], Lin-Jing Yuan[2], Yun Zhou [1], Xing-Juan Yu[1], Long Huang[3], Rong-Zhen Luo[1], Wei-Hua Jia[1] and Min Zheng[1]✉

1. Sun Yat-Sen University Cancer Center, State Key Laboratory of Oncology in South China, Collaborative Innovation Center for Cancer Medicine, Guangzhou 510060, China;
2. The First Affiliated Hospital of Sun Yat-sen University Guangzhou 510080, People's Republic of China;
3. The Second Affiliated Hospital, Nanchang University, Nanchang 330000, P. R. China.

* These authors contributed equally to this work

✉ Corresponding author: Prof. Min Zheng, M.D. Ph.D.; Address: 651 Dongfeng Road East, Guangzhou, Guangdong 510060, P. R. China; Tel: 0086 20 32968086; Fax: 0086 20 32968086; E-mail: zhengmin@sysucc.org.cn

Abstract

Myosin light chains (MLC) serve important regulatory functions in a wide range of cellular and physiological processes. Recent research found that MLC are also chromatin-associated nuclear proteins which regulate gene transcription. In this study, the MLC member myosin regulatory light chain 5 (MYL5) expression was upregulated in late stage cervical cancer patients, positively correlated with pelvic lymph node metastasis, and identified as a poor survival indicator. MYL5 overexpression promoted metastasis in cervical cancer *in vitro* and *in vivo* models, whereas MYL5 silencing had the converse effect. We demonstrated a bidirectional regulation between MYL5 and hypoxia inducible factor-1α (HIF-1α). HIF-1α activates MYL5 via binding to the hypoxia response element (HRE) in the promoter of MYL5, and MYL5 could sustain HIF-1α expression by tethering to recognition sequence AGCTCC in the HIF-1α promoter region. Clinical data confirmed a positive correlation between MYL5 and HIF-1α. In summary, our data show that MYL5 may act as a prognosis predictive factor in cervical carcinoma, and strategies that inhibit the interaction of MYL5 and HIF-1α may benefit the cervical carcinoma patients with metastasis.

Key words: MYL5; cervical cancer; oxygen regulation.

Introduction

Despite advancements in diagnostic and screening techniques and a wider availability of vaccines, cervical cancer remains the forth-leading cause of cancer-related deaths in women worldwide, with an incidence of 530,000 new cases per year [1-3]. Radical surgery and radiotherapy are potentially curative treatment for patients with early-stage cervical cancer [4]. However, a significant proportion of patients are diagnosed with local advanced disease, approximately 40% of them succumb to disease within five years [5]. Distant metastasis and local recurrence are major causes for treatment failure in these patients, making it urgent to explore new therapeutic targets by further elucidating the molecular mechanisms of cervical cancer metastasis.

Actin-dependent molecular motors, myosins, play key roles in regulating tumor progression and metastasis [6-8]. Alteration in myosin expression can be used to predict the treatment outcome and represent attractive targets for antitumor drug development in some cases [9]. On the molecular level, actin-myosin interactions are controlled by two heavy chains (MHC) and two sets of paired light chains (MLC) - the essential and the regulatory - which combine to form a long coiled-helical tail and two heads [10, 11]. The expression of MHC and MLC

members have been established as necessary for cytoskeletal dynamics and tumor cells metastasis [12]. Interestingly, recent studies showed that some myosin members, such as regulatory light chain (MLC$_{20}$, MYL9) and myosin light chain 2(MYL2), could not only affect cellular movements in the cytoplasm, but also function as transcription factors in the nucleus in certain models [13, 14].

Our previous study found that the myosin regulatory light chain 5 (MYL5) expression is decreased in cervical cancer tissues compared with the normal epithelial tissues in early stage cervical cancers [15]. The human atlas protein data showed more obvious nuclear staining of MYL5 than other MLC members in detected cancer cells. To date, however, no clinical investigation has been conducted to determine the clinical value and functional role of MYL5 in any cancer. In this study, we showed that MYL5 expression is an important indicator of an aggressive and/or poor prognostic phenotype. Overexpression of MYL5 in cervical cancer cells promotes cell invasion and metastasis both *in vitro* and *in vivo*. Moreover, we provided credence that MYL5 and hypoxia inducible factor-1α (HIF-1α) could mutually bind to each other's promoter and form a positive feedback loop to promote metastasis of cervical cancer cells, which would shed light on the new therapeutical strategies to treat this disease.

Results

Expression and clinical significance of MYL5 in cervical cancer

Gene expression microarrays from both our cancer center and a western population (NCBI/GEO DataSets/GDS3233) showed that the MYL5 expression was downregulated in early stage cervical tumor samples compared to normal tissues with a 2-fold change. (Figure S1A, B)[15]. In order to know about its clinical value in cervical cancers, we performed immunohistochemical staining for MYL5 in 197 cervical cancer tissues (stage I–II, n=167; stage III–IV, n=30) and 58 adjacent normal epithelial tissues. The results showed that MYL5 could be labelled in both the cytoplasm and nucleus of epithelial cells (Figure 1A, indicated by arrows). In contrast to normal epithelial cells, which consistently displayed moderate staining, the MYL5 expression in tumor cells varied widely (Figure 1A, B). Most early stage tumor samples showed diminished staining of MYL5 compared with the paired normal epithelial, which agreed with the microarray result (Figure S1C). However, samples from late stage (stage III–IV) patients showed obviously strong immunostaining than the early stage (stage I–II) samples (Figure 1C).

Pelvic lymph node metastasis (PLNM) is one of the important prognostic factors for cervical cancer patients. We additionally discovered that PLNM positive samples had a higher MYL5 expression than the PLNM negative samples in the 167 early stage cases (Figure 1D).

Kaplan–Meier survival analyses showed that patients with MYL5 overexpression in tumor tissues (defined as strong staining) had a shorter 5-year disease-free survival (DFS) (*P*=0.013, Figure 2A) and 5-year overall survival (OS) (*P*=0.115, Figure 2B). In addition, immunopositive staining of MYL5 in nucleus was also correlated with shorter DFS (*P*=0.020, Figure 2C) and OS (*P*=0.092, Figure 2D). Chi-square tests showed that MYL5 expression were significantly associated with distant metastasis and local recurrence (*P*=0.017, Table S1).

Influence of expression levels of MYL5 on migratory and invasive capacity of cervical cancer cells

To investigate the biofunctional role of MYL5 in cervical cancer cells, we firstly examined its expression in cervical cell lines. Compared with primary normal cervical epithelial cells (NCEC), Caski and HeLa presented a higher MYL5 expression level, whereas SiHa had a lower expression level (Figure S2). SiHa cells were stably transfected with MYL5 expression plasmid (pEZ-Lv201-MYL5) and control vector (pEZ-Lv201) respectively. The ectopic expression of MYL5 was confirmed by western blot and quantitative RT-PCR (Figure 3A). In contrast, two shRNAs targeting different MYL5 coding regions (RNAi#1 and RNAi#2), highly efficient at silencing MYL5, were stably expressed in both HeLa and Caski cell lines (Figure 3B). Cell viability was not altered by MYL5 overexpression or knockdown (Figure S3). However, MYL5 overexpression induced a three-fold to four-fold increase of the migration compared with the control cells. This effect was further examined using Matrigel invasion assays, wherein MYL5 was shown to increase the invasive capacity of SiHa cells (Figure 3C). Besides, both migratory and invasive abilities were significantly decreased when MYL5 was knockdown (Figure 3D). These results suggest that MYL5 promotes motility and invasiveness of cervical cancer cells *in vitro*.

MYL5 promotes lung colonization and lymphatic metastasis *in vivo*

To assess whether MYL5 overexpression is causative *in vivo*, animal models for hematogenous metastasis and lymph node metastasis were established using nude mice. SiHa-MYL5 cells were injected into the tail vein or footpads, while

SiHa-Vector cells were used as a control (n=6/group). Mice were sacrificed on day 45, and metastatic tumor nodules formed in the lung and popliteal lymph nodes were compared. MYL5 overexpression corresponded to an increased number of lung metastatic nodules. In the contrast, silencing MYL5 in HeLa cells significantly reduced lung metastasis (Figure 4A).

The effect of MYL5 on lymph node metastasis was investigated using a popliteal lymph node metastasis model. The SiHa-Vector, SiHa-MYL5, HeLa-RNAi-Vector, HeLa-MYL5-RNAi#2 cells were inoculated into the footpads of nude mice (n=6/group; Figure 4B). The popliteal lymph nodes were enucleated and analyzed after 45 days. Lymph nodes from MYL5-transduced cells displayed higher numbers of cytokeratin-positive tumor cells than tumors formed from control cells (Figure 4C). Conversely, the lymph node formed from MYL5-silenced cells had less cytokeratin-positive tumor cells than vector control tumors (Figure 4C). Strikingly, the metastatic to total ratios of dissected popliteal lymph nodes were markedly higher in the SiHa-MYL5 group (100%) than in the control group (50%) (Figure 4D); in contrast, the metastatic to total ratios of dissected popliteal lymph nodes in MYL5-silenced groups were markedly reduced, from 66.7% to 16.7% (Figure 4D). In summary, these observations showed that MYL5 promotes cervical cancer cell metastasis *in vivo*.
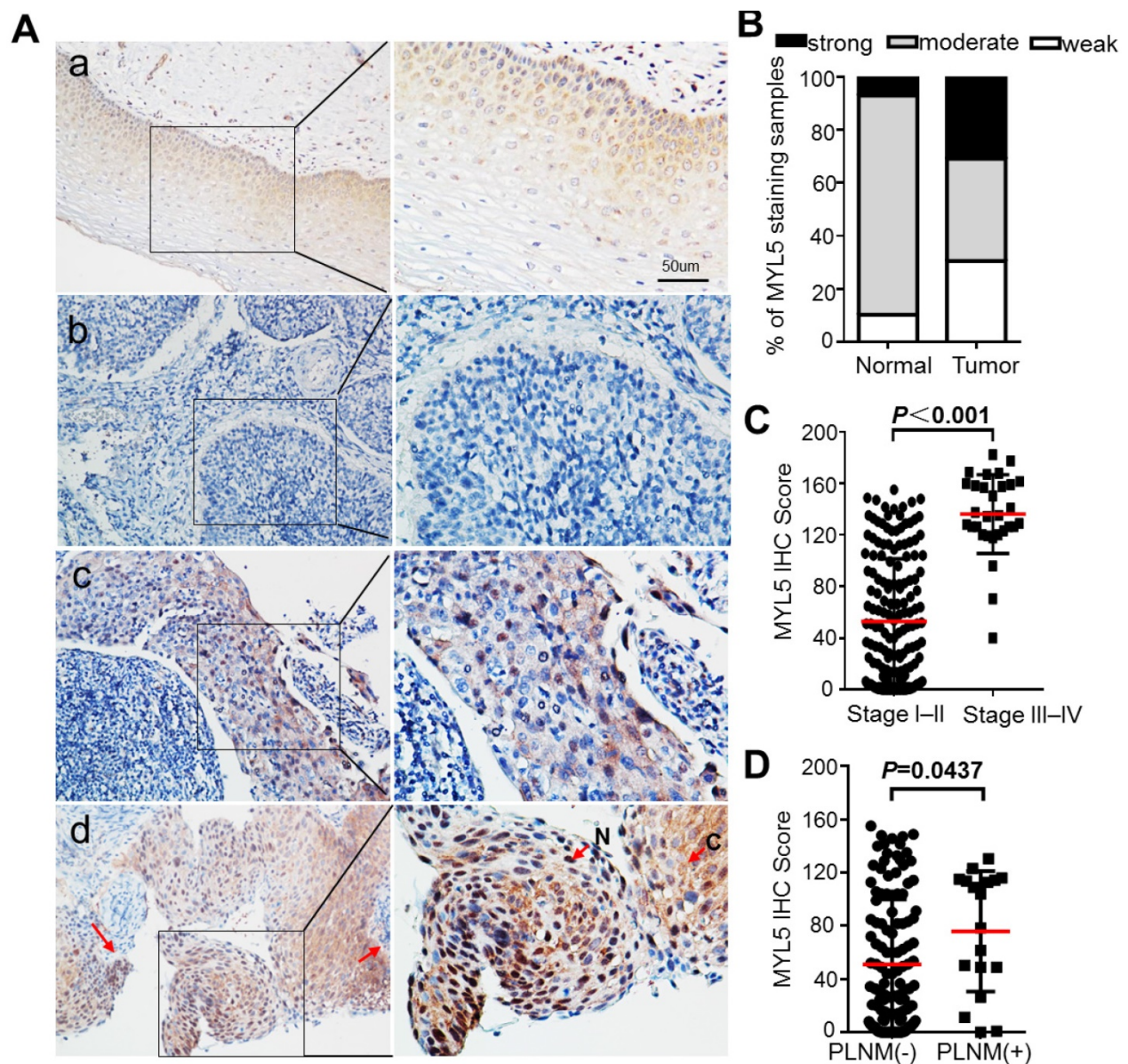

Figure 1. Expression of MYL5 in cervical cancers. A. Representative images of MYL5 staining in cervical normal epithelial tissues (a) and images of negative (b), moderate (c), strong (d) MYL5 staining in the tumor tissues. The abbreviation C and N denote cytoplasmic and nuclear location of MYL5. Bar=50μm. **B.** MYL5 quantifications on 196 samples of human cervical cancer. **C.** Immunostaining analysis indicates higher MYL5 expression in late stage patients. **D.** MYL5 in PLNM-positive tissues is significantly higher than that in PLNM-negative tissues. PLNM: pelvic lymph node metastasis.
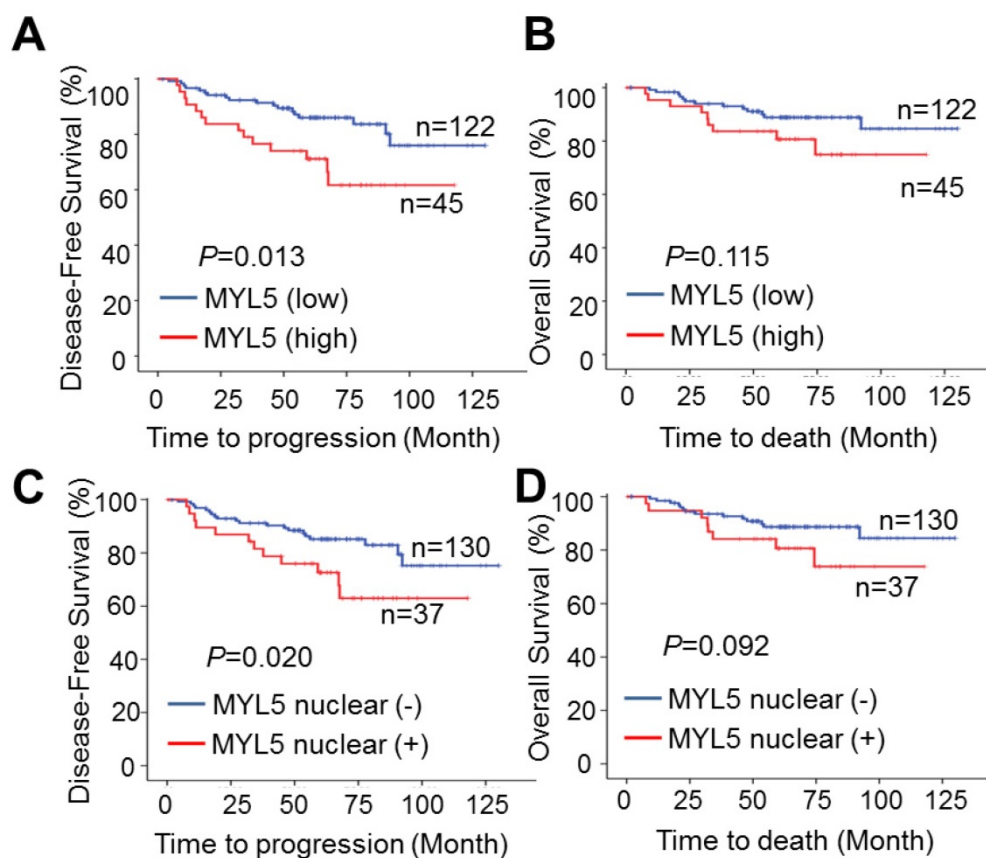
Figure 2. MYL5 expression is associated with poor survival in cervical cancer patients. A. High MYL5 protein expression correlates with shortened disease-free survival. **B.** Kaplan-Meier plots of overall survival rate of cervical patients stratified by MYL5 expression. **C.** Positive MYL5 nuclear protein expression correlates with shortened disease-free survival. **D.** Kaplan-Meier plot of overall survival rate of cervical cancer patients according to MYL5 nuclear protein expression. *P* value was calculated by log rank test.

MYL5 upregulates HIF-1α in cervical cancer cells

Since MYL5 was present in the nucleus of cells, we wondered whether MYL5 could induce gene expression changes in cervical cancer cells. Using a Aligent SurePrint G3 Human GE 8×60K Microarray, we found that genes associated with cellular metabolic process and cell motility changed significantly in MYL5 overexpressing cells compared with control cells (Figure S4). Hypoxia inducible factor 1α (HIF-1α), one of the key transcription factor in regulating cancer cell metabolism and metastasis [16], was increased by 1.6-fold in MYL5 overexpressed cells (Figure 5A). Quantitative RT-PCR analysis demonstrated higher expression of HIF-1α mRNA levels after transient transfection of MYL5 in SiHa cells. On the other hand, HIF-1α mRNA levels were decreased when MYL5 was silenced (Figure 5B). Western blot demonstrated that MYL5 could regulate HIF-1α expression in both normoxia and hypoxia conditions (Figure 5C). Furthermore, when we added a classical nuclear location signal (NLS) sequence on the 3' end of MYL5 coding sequence for delivering MYL5 directly to the nuclear (Figure S5A, B), both the HIF-1α expression and the cell migration ability were further increased (Figure S5C, D), suggesting that it is the nuclear fraction of MYL5 to contribute the regulation of HIF-1α expression and associated cell migration.

To further investigate whether MYL5 could regulate HIF-1α transcript directly, we generated a reporter construct (pGL3-HIF-1α) with luciferase gene driven by HIF-1α promoter (-2000bp to +143bp). Luciferase reporter assay showed that luciferase activity driven by the HIF-1α promoter was heightened in MYL5-transduced cells compared with control cells (Figure 5D), suggesting possible regulation of HIF-1α transcription by MYL5 via binding to the HIF-1α promoter region. Previous studies reported that the AGCTCC sequence could be recognized and tethered by myosin light chain proteins [13, 14]. We found that there exists the AGCTCC sequence in the promoter region of HIF-1a next to the transcriptional start site. ChIP assay was performed in Flag-MYL5 overexpressing HeLa cells. Results showed that MYL5 could bind to the AGCTCC region of HIF-1α promoter (Figure 5E).
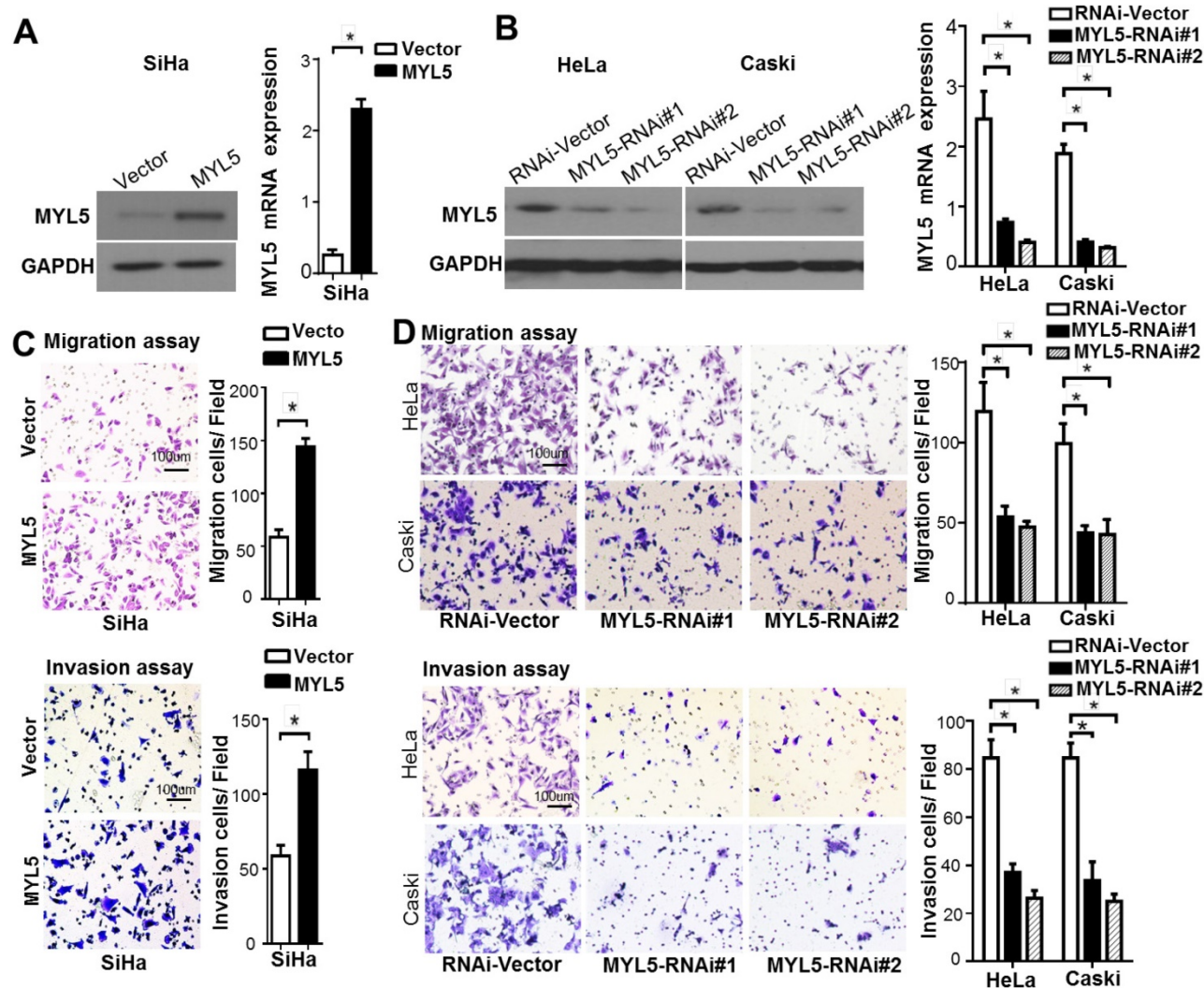
Figure 3. MYL5 increases cell migration and invasion *in vivo*. A. Western blot and quantitative RT-PCR demonstrate ectopic overexpression of MYL5 in SiHa cells. **B.** Western blot and quantitative RT-PCR demonstrate downregulation of MYL5 in HeLa and Caski cells as a result of shRNA stable transfected. **C.** Overexpression of MYL5 promotes SiHa cell migration and invasion. **D.** Decrease MYL5 inhibits cell migration and invasion in HeLa and Caski cells. Left panel shows representative transwell cell migration and matrigel cell invasion images. Right panel shows quantified migration and invasion capacities. The data represented are shown as means±s.e.m. collected from 6 fields of 3 independent experiments. Bar=100μm. *P<0.05 by Student's t-test.

To confirm that MYL5-induced HIF-1α was functionally active, the expression levels of known HIF-1α downstream genes were detected by quantitative RT-PCR between MYL5 overexpression cells and control cells. We observed that expression levels of all genes were significantly increased in MYL5 overexpressed cells (*P*<0.05) (Figure 5F).

Bidirectional regulation between MYL5 and HIF-1α

It is well established that Hypoxia inducible factors (HIFs) bind to hypoxia response elements (HRE) with consensus sequence 5'-A/GCGTG-3' in the promoter of the genes they regulate [17]. In silico analysis identified that MYL5 promoter (−3000bp to +50bp) contained 4 putative HREs (Figure 6A). Therefore, we investigated whether MYL5 could be induced under hypoxia condition or regulated by HIF-1α. Results showed significant increase of MYL5 mRNA and protein levels in all cervical cell lines under hypoxic stress (1% O$_2$), compared with normoxic condition (20% O$_2$) (Figure 6B). Overexpression of HIF-1α increased MYL5 expression, inferring that HIF-1α is a regulatory factor of MYL5 (Figure 6C). Additional study found that MYL5 could be increased by hypoxia, even when endogenous HIF-1α was silenced by interference RNA (Figure 6D), suggesting that HIF-1α is not the exclusive regulatory factor for MYL5 expression. Next, we performed a chromatin immunoprecipitation (ChIP) assay to verify the effective binding site of these putative HREs. HIF-1α antibody was used to immunoprecipitate HIF-1α bound DNA. We then used primers targeted 4

different HRE containing areas to quantify the amount of DNA that was immunoprecipitated by HIF-1α. The results showed that HIF-1α ChIPs were enriched for the primer set 4, indicating that HIF-1α bind to this site in the promoter of MYL5 (Figure 6E).

To shed further light on the relation of MYL5 with the regulation of HIF-1α, an immunohistochemistry analysis was conducted to examine the expression of HIF-1α in 96 cervical cancer specimens. An association study concluded that expression of MYL5 positively correlated with HIF-1α ($P<0.001$). The following quantitative RT-PCR in 45 primary cervical cancer specimens demonstrated the positive correlation between MYL5 with HIF-1α ($R=0.550$, $P<0.001$, Figure 6F).

Potential therapeutic value of the inhibition of MYL5

Studies implicate regulatory functions of hypoxia in each step of tumor metastasis, such as epithelial-mesenchymal transition (EMT), invasion, extracellular matrix (ECM) modulation and cell motility et al [18]. Antiangiogenic drug, which is the only target agent approved for the treatment of persistent, recurrent or late-stage cervical cancer [19, 20], are observed to increase invasiveness and metastasis of tumor cells in preclinical models [21, 22],

one mechanism of which is that the neovascularization blocking induced hypoxia. Therefore, agents targeting the function of hypoxia or inhibiting the expression of HIF-1α may potentially reduce tumor-intrinsic and treatment-induced metastasis [18, 23, 24]. We found that knockdown of MYL5 inhibit cell migration potential in HIF-1α overexpression cells or under hypoxic condition (Figure 7A, B), suggesting MYL5 pertains to an active role in hypoxia-induced cell motility. Notably, *in vivo* results showed that silencing MYL5 significantly reduced lung metastasis, and number of cytokeratin-positive tumor cells in lymph nodes mediated by HIF-1α in transfected mice (Figure 7C). Additionally, the metastatic to total ratios of dissected popliteal lymph nodes were also markedly reduced, from 100% to 50% (Figure 7D, E). Therefore, inhibition of MYL5 may possess potential therapeutic value.

Discussion

Myosins were traditionally thought to function within the cytoplasm, some studies now stipulate multiple myosins as being present in the nucleus [25, 26]. The presence of myosin II, such as MLC_{20}, MYL2, in the nuclei of several cell types, and their transcriptional function is gradually reported [13, 14]. However, little is known about the presence and
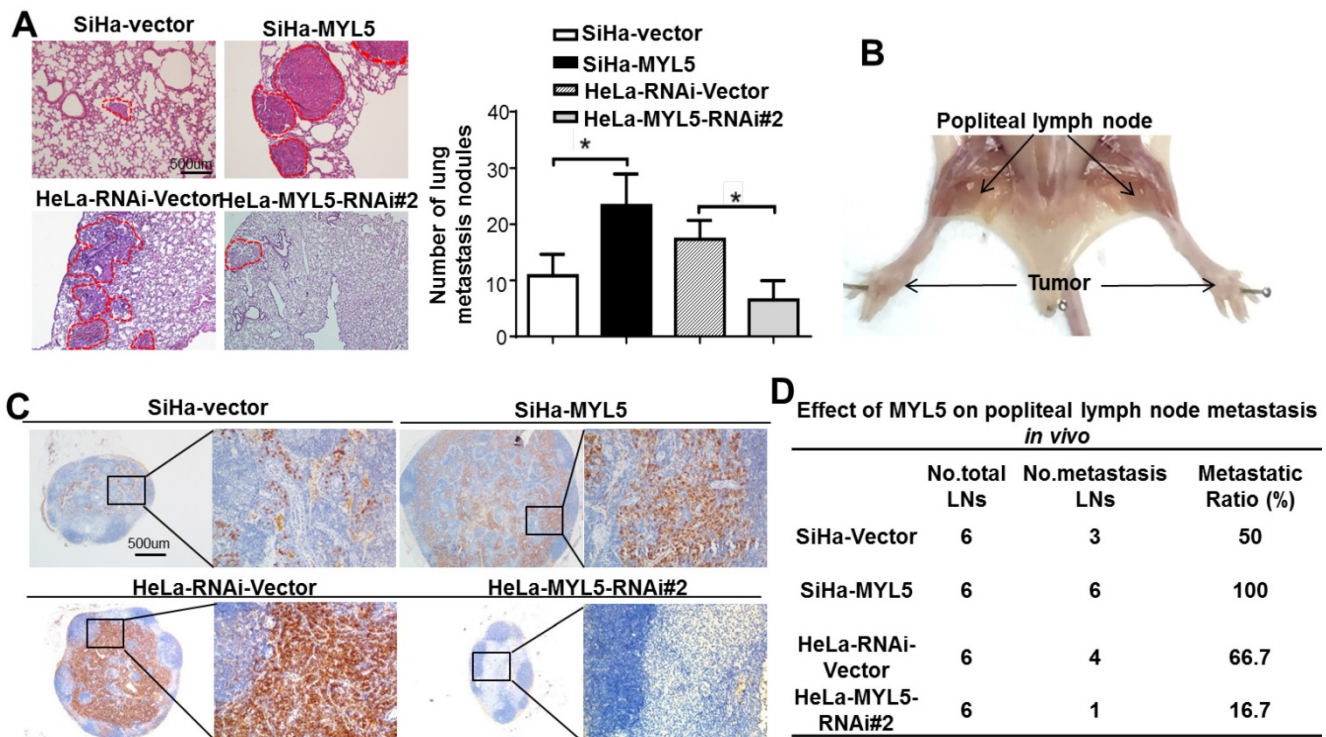

Figure 4. MYL5 promotes tumor metastasis *in vitro*. A. An experimental mouse model was used to evaluate the effect of MYL5 on tumor metastasis by tail vein injection of SiHa-Vector, SiHa-MYL5, HeLa-RNAi-Vector, HeLa-MYL5-RNAi#2 cells. Representative H&E stained lung sections and number of lung metastatic nodules in tested mice (n=6). Bar=500μm. The number of metastatic nodules formed in the lungs is summarized in the right panel. **B.** A popliteal lymph node metastasis model was established in BALB/c nude mice and analyzed. **C.** Representative images of popliteal lymph nodes immunostained with anti-cytokeratin antibody from mice inoculated with indicated cells. Bar=500μm. **D.** Ratios of metastatic to total dissected popliteal lymph nodes from mice inoculated with indicated cells. *$P<0.05$.

Effect of MYL5 on popliteal lymph node metastasis *in vivo*

	No.total LNs	No.metastasis LNs	Metastatic Ratio (%)
SiHa-Vector	6	3	50
SiHa-MYL5	6	6	100
HeLa-RNAi-Vector	6	4	66.7
HeLa-MYL5-RNAi#2	6	1	16.7

function of the MLC member MYL5, which was demonstrated an altered expression gene in cervical cancer. In this study, we show that MYL5 can be detected in both cytoplasm and nucleus of cervical cells. Clinical dataset analyses suggest that MYL5 affects cervical cancer patient prognosis. A combination of *in vitro* cellular system, and multiple *in vivo* metastasis models show that gain of MYL5 promotes metastatic progression. Conversely, loss of MYL5 suppresses metastasis, and is of potential therapeutic value. Furthermore, functional and mechanistic studies of MYL5 suggest a critical role of MYL5 in the control of cell metastasis via interacting with HIF-1α (Figure 7F).

Hypoxia is a predominant feature in cervical cancer, as well as a wide range of solid tumor [27, 28]. It regulates each step of the tumor metastasis process, from the initial EMT to the ultimate organotropic colonization [16, 18]. High level of intra-tumor hypoxia, followed by stabilization and activation of the HIF-1α may induce EMT through activating certain specific transcription factors, such as Snail1, Snail2, ZEB1, TWIST, and activate EMT-associated signaling pathway, such as transforming growth factor-β and Notch pathways. In addition to EMT, hypoxia can activate many other sequences of metastasis. Hypoxic stress causes angiogenesis

through multiple pathways. The antiangiogenic antibody bevacizumab is an agent approved for the treatment of persistent, recurrent or late-stage cervical cancer, based on increased survival statistics from clinical trials [19, 20]. However, studies showed that cancer patients' preclinical models rapidly become resistant, with a short remission before progression after antiangiogenic therapy. One cause of this may be increased hypoxia in tissue, which likely promotes tumor recurrence locally and at distant sites [29, 30]. Hypoxia can fuel resistance to treatment by promoting genomic instability, angiogenesis and invasion [31]. Therefore, targeting hypoxia through different approaches at appropriate time windows may drastically reduce tumor-intrinsic and treatment-induced metastasis [18, 24].

Our gene microarray results showed that cancer metabolism and metastasis associated genes upregulated obviously in MYL5 overexpressing cells, and HIF-1α increased with 1.6-fold. Quantitative PCR and western blot confirmed the upregulation of HIF-1α when MYL5 was overexpressed. Previous studies reported the MLC members MYL9 and MYL2 could tether to sequence AGCTCC in the promoter of ICAM-1 or NOX2, and upregulate these genes expression in human colonic circular smooth muscle cells and myocardium cells respectively [13, 14].
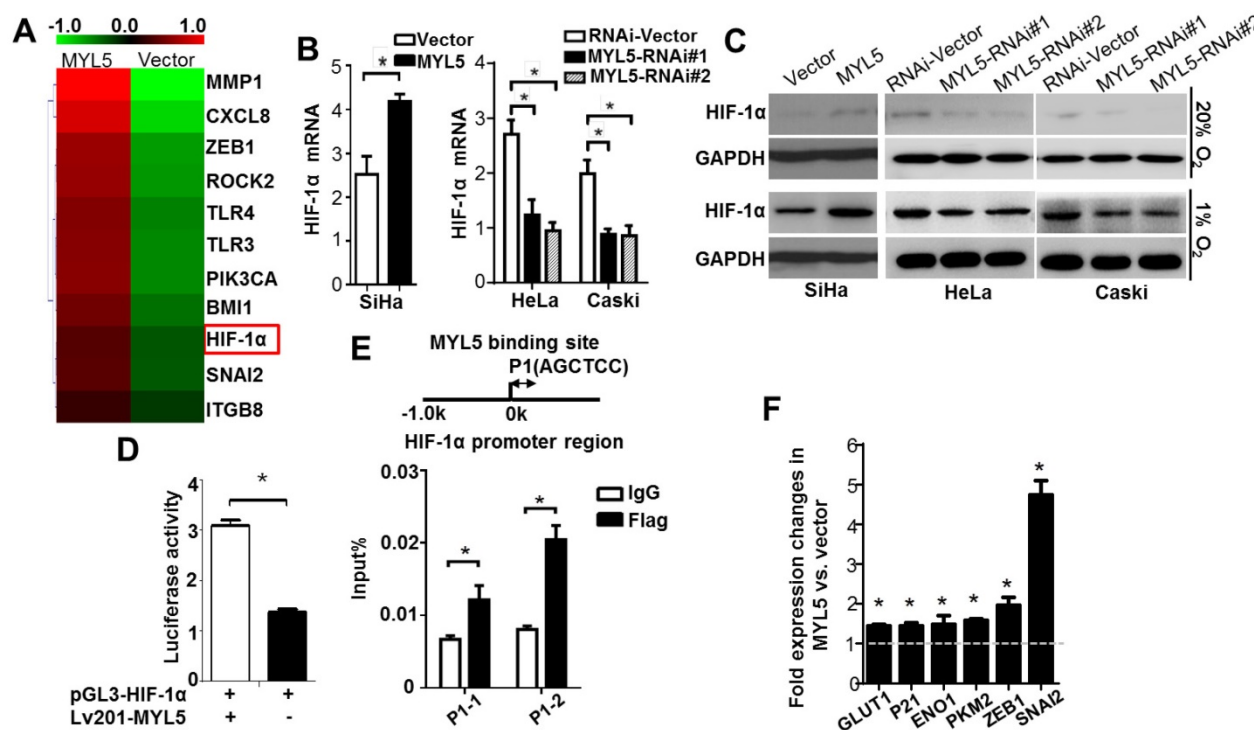

Figure 5. MYL5 upregulates HIF-1α in cervical cancer cells. A. Heat map showing differentially expressed genes in MYL5 overexpressing SiHa cells and control cells. **B.** Quantitative RT-PCR analysis of HIF-1α mRNA expression in the indicated cells. **C.** Western blot of HIF-1α protein levels in the indicated cells. **D.** Fragments encompassing the putative HIF-1α promoter region (−2000bp to +143bp) were inserted upstream of firefly luciferase coding sequences in the pGL3-basic plasmid. pGL3-HIF-1α was co-transfected with lv201-MYL5 and pTK-Renilla into SiHa cells. Co-transfected with empty vector was used as a control. The ratio of Fluc to Rluc activity is shown as mean±s.e.m. of 3 independent experiments. **E.** ChIP analysis of MYL5 binding on HIF-1α promoter. Sheared chromatin was immunoprecipitated using ChIP-grade anti-Flag antibody or IgG control. **F.** Expressions of 6 HIF-1α regulated genes were compared by quantitative RT-PCR between SiHa-MYL5 and SiHa-Vector cells. Error bars represent the mean±s.e.m. of three independent experiments. *P＜0.05.

When we found that there also exists the AGCTCC sequence in HIF-1α promoter region, we decided to test whether MYL5 could upregulate HIF-1α by binding to its promoter. ChIP and luciferase activity assays indicated that MYL5 could directly bind to this sequence in HIF-1α promoter. Interestingly, our study also found that both hypoxia condition and HIF-1α overexpression could enhance MYL5 expression. The bidirectional regulation between MYL5 and HIF-1α forms a positive feedback to promote the progression of cervical cancer cells. The gene microarray results

suggested that MYL5 may target other metastasis-associated genes such as ROCK2 besides HIF-1α. Therefore, inhibiting MYL5 could be good choice to reduce metastasis with or without relationship to HIF-1α. We observed that the depletion of MYL5 could inhibit cancer cell migration under hypoxia conditions and reduce metastasis induced by HIF-1α *in vivo*. We speculate that an addition of MYL5-silencing treatment could decrease antiangiogenic therapy induced metastasis in cervical cancer.
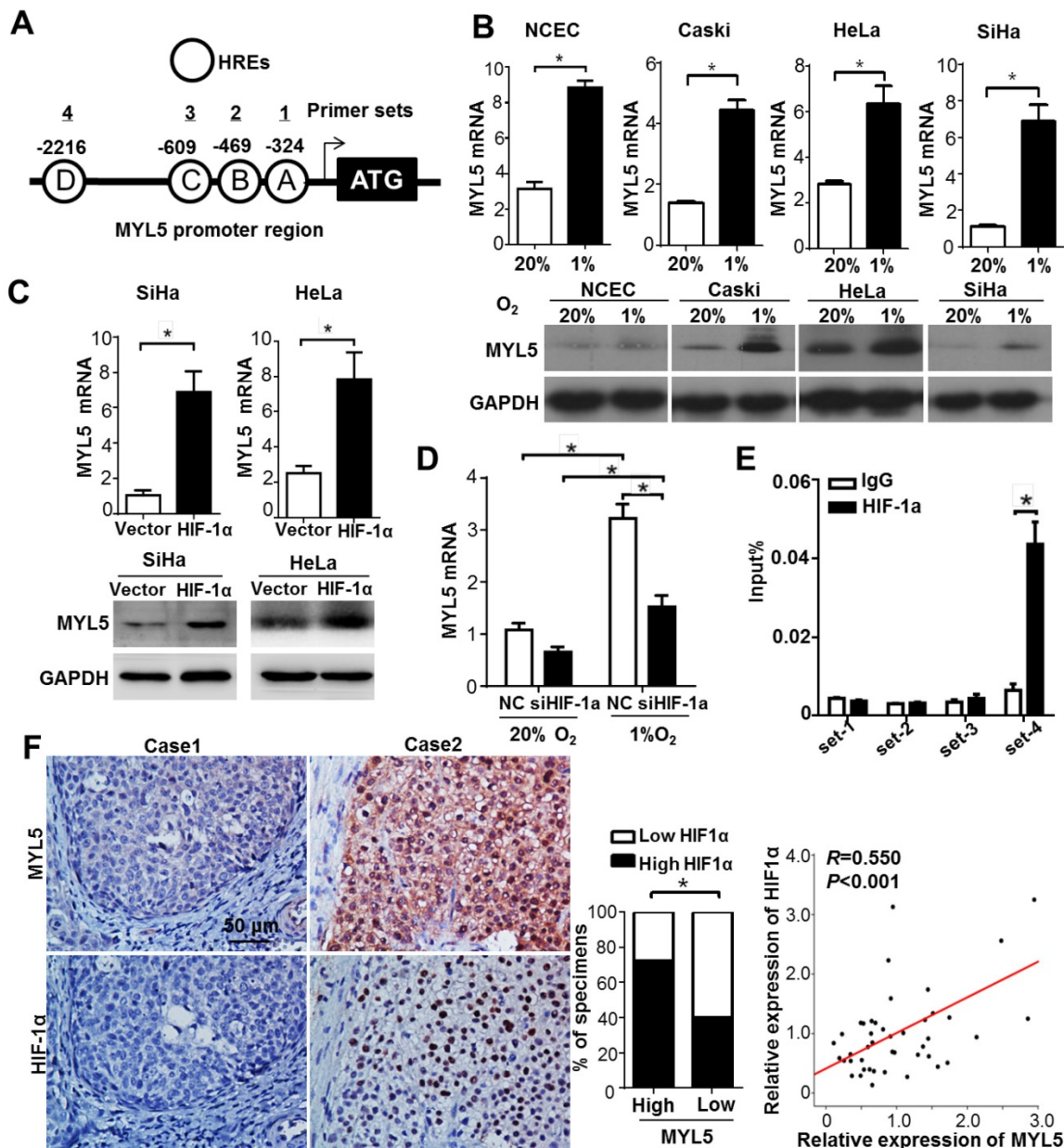

Figure 6. Bidirectional regulation between MYL5 and HIF-1α A. Schematic illustration of MYL5 promoter. Each circle labeled with a letter represents a putative HRE and the location of each HRE is labeled above. Each numbered line above shows the location of a primer pair designed to amplify a region of DNA with specific putative HREs in a ChIP. **B.** Expression of MYL5 was compared between cells cultured under normoxia (20% O_2) and hypoxia (1% O_2) condition in 4 cervical cell lines by quantitative RT-PCR and western blot. **C.** Levels of MYL5 in HIF-1α overexpressing cells were determined by quantitative RT-PCR and western blot. **D.** The mRNA levels of MYL5 in SiHa cells exposed to normoxia and hypoxia after HIF-1α were silenced. **E.** ChIP analysis of HIF-1α binding on MYL5 promoter. ChIP DNA was quantified by real-time PCR primers specific to human MYL5 promoter. **F.** MYL5 levels positively correlated with HIF-1α in cervical cancer specimens. Left panel, images of two representative cases. Bar=100μm. Middle panel, percentages of cervical cancer specimens with low or high expression of MYL5 relative to HIF1α expression. Right panel, correlation analyses between the mRNA expression of MYL5 and HIF1α in 45 freshly collected cervical samples. Error bars represent the mean±s.e.m. of three independent experiments. *$P < 0.05$.
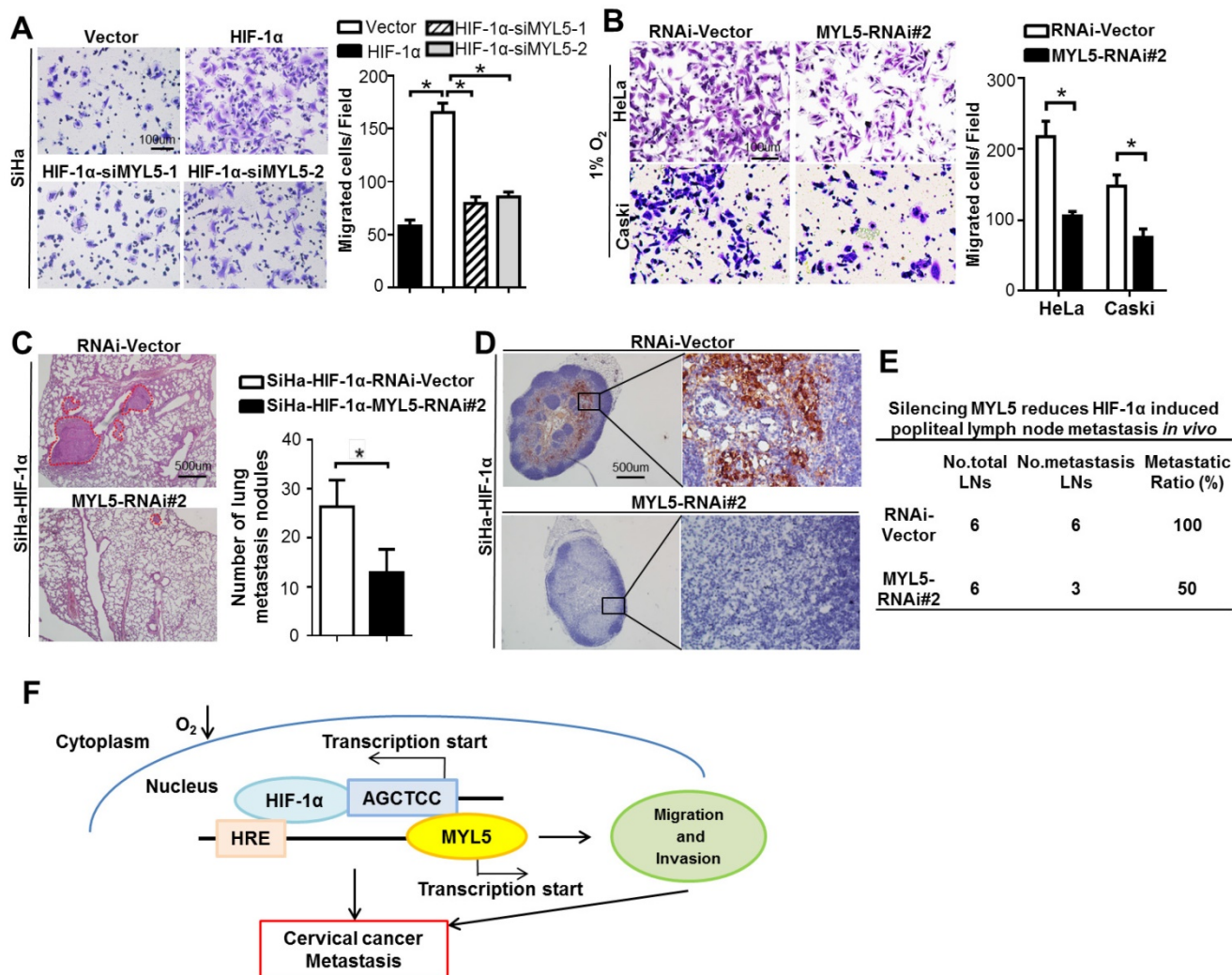
Figure 7. Potential therapeutic value of the inhibition of MYL5. A. Knockdown of MYL5 with interference RNA decreased HIF-1α induced cell migration. Left panel shows representative images of cell migration. Right panel shows quantified migration capacities. Bar=100μm. **B.** Knockdown of MYL5 inhibited hypoxia induced cell migration. Left panel shows representative images of cell migration. Right panel shows quantified migration capacities. Bar=100μm. **C.** Representative H&E stained lung sections and quantification indicating numbers of lung metastatic nodules in tested mice (n=6). Bar=500μm. **D.** Representative images of popliteal lymph nodes immunostained with anti-cytokeratin antibody from mice inoculated with the indicated cells. Bar=500μm. **E.** Ratios of metastatic to total popliteal lymph nodes dissected from mice inoculated with indicated cells. Error bars represent the mean ±s.e.m. of three independent experiments. *$P < 0.05$. **F.** Molecular mechanism between MYL5 and HIF-1α under hypoxia condition.

As the MLC member MYL9 and MYL2 also have the putative binding site sequence AGCTCC, we wonder the regulation of HIF-1α is MYL5 special or the MLC general function. We examined the MYL9 protein in 30 cases of cervical cancer, the results showed significant differences between MYL5 and MYL9. MYL9 immunohistochemistry staining occurred mainly in the stroma cells such as the fibroblast, and in the cytoplasm of tumor cells (Figure S6). No nuclear staining can be found. However, MYL5 can be detected in epithelial cells' cytoplasm and nucleus. Similarly, there is no nuclear staining of MYL2 in common cancer cells according to the human protein atlas data. The role and function between MYL5 and other MLC members may be quite different according to their different cell location in cervical cancers.

In summary, MYL5 is a metastasis-promoting gene, which has significant value to predict postoperative recurrence for patients with cervical cancers. Exploring the genes regulated by MYL5 will provide further clues to its biological roles and more generally will contribute to the understanding of myosin light chains, and the mechanisms underlying the metastasis of cervical cancer.

Materials and Methods

Cervical cancer patients and cancer tissue samples

Archived, formalin-fixed, paraffin-embedded tissues were obtained from 197 patients who

diagnosed with cervical cancer at the Sun Yat-Sen University Cancer Center, including 167 patients with stage I-II who underwent surgical resection and postoperative chemotherapy or radiation if pathologic risk factors are discovered between 2000 and 2008, 30 patients with stage III- IV who underwent cervical biopsy between 2015 and 2016 at the Sun Yat-Sen University Cancer Center. The inclusion criteria used in patient enrollment were absence of anticancer therapies prior to the treatment. The clinicalpathological characteristics of the patients are summarized in Supplementary Table S1. All patients with stage I-II attended follow-up visits at the outpatient clinic with regular surveillance for recurrence using history and physical examination, the serum squamous cell carcinoma antigen level for patients with squamous cell carcinomas, pelvic and abdominal ultrasonography, and chest radiography at 3- to 6- month intervals. When tumor recurrence or metastasis was suspected, further examinations, including CT and PET-CT scan were performed. Biopsies were taken when necessary. Patients with confirmed recurrence received further treatment, including surgical resection, local ablative therapies, concurrent chemotherapy with or without radiotherapy. Of the 167 patients who were examined using the immunochemistry analysis, the median follow-up was 63.1months (range 1-130 months), 22 patients (13.2%) died, 32 patients (19.2%) were diagnosed with tumor recurrence. The disease-free survival (DFS) was defined as the interval between surgery and recurrence or between surgery and the last observation for patients without survival (for censored observations). Overall survival (OS) was defined as the interval between surgery and death or between surgery and the last observation for surviving patients (for censored observations). Staging was carried out according to the International Federation of Gynecology and Obstetrics (FIGO 1994) classification guidelines. Two experienced pathologists performed the grading and histopathological subtyping of specimens, based on World Health Organization criteria. Human samples used in this study were approved by the Sun Yat-Sen University Cancer Center Medical Ethics Committee. Written informed consent was obtained from all patients.

Cells lines

Primary normal cervical epithelial cells (NCEC) were established by isolating and mincing cervical epithelial tissue from surgically-removed benign uterine disease and cultured in CELLBIND surface bottles (Corning Incorporated, NY, USA) with Keratinocyte/serum-free medium (Life Technology)

(Figure S7). The human cervical cancer cell lines HeLa, SiHa, Caski and the human kidney cell line HEK-293T were obtained from the Cell Bank, Shanghai Institutes for Biological Sciences (Shanghai, China). Cells were grown in RPMI-1640 medium (Gibco BRL, San Francisco, CA, USA), supplemented with a 10% fetal bovine serum (HyClone, Logan, Utah, USA).

RNA extraction and real-time qRT-PCR

Total RNA from cultured cells and fresh frozen cervical tissues was extracted using Trizol reagent (Life Technology), according to the manufacturer's instructions. Reverse transcriptase reactions using MMLV reverse transcriptase reagents (Promega Corporation, Madison, WI, USA) were performed following manufacturer's protocol. Gene expression levels were normalized to house-keeping gene β-actin and GAPDH. Reactions were performed in triplicate with the Roche LightCycler 480 II PCR system (Roche Diagnostics, Rotkreuz, Switzerland). Primer sequences are listed in Supplementary Table S2.

Western blotting

Protein was extracted using the protein extraction kits (KeyGen Biotech, KGP150 and KGP250, Nanjing, China). Protein samples were treated with Dual Color Protein Loading Buffer (Thermo Fisher Scientific) containing reducing agent at 95°C for 10 min, resolved on 10% Tris-HCl polyacrylamide gels, and transferred to a polyvinylidene fluoride membrane. Overnight incubation (4°C) of the primary antibody was followed by HRP-conjugated antibody and Immobilon Western Chemiluminescent HRP Substrate (Millipore Corporation, Billerica, USA). A detailed list of antibodies used can be found in Supplementary Table S3.

Immunohistochemistry, automated image acquisition and quantification of immunohistochemistry staining

Immunohistochemistry was carried out using a 2-step protocol (DakoCytomation, Glostrup, Denmark). Post dewaxing, hydration and endogenous peroxidase blocking was carried out (0.3% H_2O_2 for 10 min). Antigen retrieval was performed by steaming sections in 10mM citrate buffer for 10 min. Sections were incubated overnight at 4°C with rabbit anti-human MYL5, rabbit anti-human SLUG, or rabbit anti-human HIF-1α. Isotype antibody staining was used as negative control. Horseradish peroxidase-conjugated anti-mouse and anti-rabbit Dako EnVision systems (DakoCytomation) were used as secondary detection reagents and developed with

3,3'-diaminobenzidine (DAB).

To detect and evaluate the MYL5 signal in cervical cancers without bias, we established an automated and standardized quantification method using the Vectra-Inform image analysis system (Perkin-Elmer Applied Biosystems, Foster City, CA). Stained sections were captured with the Nuance VIS-FL Multispectral Imaging System and analyzed with the InForm 2.0.1 image analysis software (Perkin-Elmer Applied Biosystems). A spectral unmixing algorithm separated the grayscale images representing each spectral component quantitatively. The InForm software enabled tissue compartment (tumor tissue, peritumoral stroma tissue, blank) and cell compartment (cytoplasm, nucleus) segmentation. The DAB object density counts per megapixel for each tissue category were used for further analysis (Supplementary Figure S8).

RNA interference

Short interfering RNA designated specifically against MYL5 and HIF-1α and corresponding scrambled siRNA were purchased (GenePharma, Suzhou, China). The sequences were summarized in Supplementary Table S4. For transfection, 4ug siRNA were dissolved in 250ul of Optimem media (Life Technology). In another tube, the transfection medium Lipofectamine 2000 reagent (Life Technology) was dissolved in 250ul of Optimem media. The 2 mixtures were then combined and incubated for 20 minutes at room temperature. The mixture was added to 5×10^5 cells re-suspended in 2ml of serum-free media, plated in a 6-well plate and incubated for 5 hours at 37°C. After transfection, the medium was replaced with normal growth medium containing 10% fetal bovine serum. Cells were harvested at 48 hours, and the effect of gene silencing was examined by western blot.

Plasmid constructs and lentiviral infection

The pEZ-lv201-MYL5, pEZ-lv203-Flag-MYL5, pEZ-lv105-HIF-1α, psi-LVRH1MP-MYL5-RNAi#1, psi-LVRH1MP-MYL5-RNAi#2 plasmids and the respective control plasmids were purchased from GeneCopoeia (FulenGen, Guangzhou, China) and transfected into the 293FT packaging cell line using a Lenti-Pac™ HIV Expression Packaging Kit (GeneCopoeia, Inc) according to the manufacturer's instructions. Virus-containing supernatants from 293FT cells were collected and then filtrated using 0.45- μm filters. The filtered supernatant was added to 70% confluent cells in the presence of 8 μg/ml polybrene (Sigma, St. Louis, MO, USA). After 48 hours, the cells were incubated with fresh complete medium containing the appropriate concentration of

puromycin for stable transduced cells. The HIF-1α promoter (−2000 ~ +143) was provided by Professor Li Yan at Sun Yat-Sen University Cancer Center. The sequence of NLS is PAAKRVKLD [32]. MYL5 gene was cloned into pSin vector to construct pSin-MYL5 and the NLS sequence was tagged on the 3' end of MYL5 coding sequence to construct pSin-MYL5-NLS expression vector. Successful cloning was confirmed by DNA sequencing.

Migration and invasion assays

For transwell migration assays, 10^5 cells were placed in top chamber of each insert (BD, Durham, NC, USA). For invasion assays, 10^5 cells were plated on a transwell chamber coated on the inside with 1:4 diluted Matrigel (BD Biosciences, Bedford, Massachusetts, USA) in the insert of a 24-well culture plate. Medium containing 10% fetal bovine serum was added to the lower chamber as a chemoattractant. After 6 h or 8 h (for migration assay) and 48h (invasion assay) in the CO_2 incubator, cells inside the chamber were gently removed with a cotton swab. Migration cells located on the lower side of the chamber were stained with crystal violet, air dried and photographed. Three independent experiments were performed and data are presented as the mean ± s.e.m.

Chromation immunoprecipitation assay

Cells were grown to 90% confluence and cells were then treated with 1% formaldehyde to cross-link proteins to DNA. The crosslinking, immunoprecipitation, washing, elution, reverse crosslinking, and proteinases K treatment were performed according to the manufacturer's directions described in the SimpleChIP Enzymatic Chromatin IP Kit #9003 (Cell Signaling Technology, Inc). Antibodies used were listed in Supplementary Table S3. Purified immunoprecipitated DNA was used for real time qPCR. Primers for ChIP PCR are shown in Supplementary Table S5.

Luciferase assay

Briefly, 1×10^4 cells per plate were seeded in 24-well plates in triplicate, and allowed to settle for 12h. SiHa cells were transfected with pGL3-basic, pGL3-ctrl, or pGL3-HIF1a promoter fragments and pTK-Renilla, together with the MYL5 expression vector or vector control using the Lipofectamine 2000 reagent. Luciferase and renilla signals were measured 48h after transfection using the Dual Luciferase Reporter Assay Kit (Promega Corporation), according to the manufacturer's protocol.

Animal experiments

Female nude BALB/c-nu mice (4-5 weeks of age,

18-20g) were purchased from the Center of Experimental Animals of Guangdong. Animal experiments were carried out in compliance with the Welfare of Experimental Animals guidelines at Sun Yat-Sen University. As for the lymph node metastatic mouse model, the BALB/c-nu mice were randomly divided into four groups (n=6/group) and injected subcutaneously with 1.5×10^5 cells (SiHa-vector/ SiHa-MYL5; HeLa-RNAi-Vector/HeLa-MYL5-RNAi#2) into the footpad as previously described [33]. After 45 days, the tumors and popliteal lymph nodes were excised and measured. Serial 4.0μm sections were obtained analyzed by immunostaining with anti-SLUG and anti-cytokeratin antibodies. The popliteal lymph nodes were estimated using the equation $(L \times W^2)/2$. The ratios of positive-stained lymph nodes to total lymph nodes were calculated. To generate the lung metastasis mouse model, the BALB/c-nu mice were randomly divided into four groups (n=6/group). Animals received 5×10^5 cells (SiHa-vector/SiHa-MYL5; HeLa-RNAi-Vector/HeLa-MYL5-RNAi#2) in PBS through tail vein and were sacrificed after 45 days, tissues of lung were isolated and paraffin embedded for further routine histology examination by hematoxylin and eosin stain.

Statistical analysis

Statistical analysis was performed using a SPSS software package (SPSS Standard version 16.0, SPSS Inc) and GraphPad Prism software (version 6, GraphPad Software, CA, USA). The association between various clinical characteristics and expression levels of MYL5 was examined by the chi-square test or by Fisher's exact test. PFS and OS were examined by Kaplan-Meier analysis. A log rank test was used to compare different survival curves. Multivariate survival analysis was performed on all parameters that were found significant in univariate analysis using the Cox regression model. Data derived from cell-line experiments are presented as mean±s.e.m. and assessed by a two-tailed Student's t-test. *P* values ＜0.05 were considered significant.

Abbreviations

MLC, myosin light chains; MYL5, myosin regulatory light chain 5; HIF-1α, hypoxia inducible factor-1α; HRE, hypoxia response element; MHC, myosin heavy chains; PLNM, pelvic lymph node metastasis; EMT, epithelial-mesenchymal transition; NCEC, normal cervical epithelial cells; DFS, disease free survival; OS, Overall survival; FIGO, international federation of gynecology and obstetrics.

Supplementary Material

Supplementary figures and tables.
http://www.thno.org/v07p3768s1.pdf

Competing Interests

The authors have declared that no competing interest exists.

References

1. Crosbie EJ, Einstein MH, Franceschi S, Kitchener HC. Human papillomavirus and cervical cancer. Lancet. 2013; 382: 889-99.
2. Isidean SD, Franco EL. Embracing a new era in cervical cancer screening. Lancet. 2014; 383: 493-4.
3. Forouzanfar MH, Foreman KJ, Delossantos AM, Lozano R, Lopez AD, Murray CJ, et al. Breast and cervical cancer in 187 countries between 1980 and 2010: a systematic analysis. Lancet. 2011; 378: 1461-84.
4. Zheng M, Huang L, He L, Ding H, Wang HY, Zheng LM. Evaluation of the effects of type II radical hysterectomy in the treatment of 960 patients with stage IB-IIB cervical carcinoma: A retrospective study. J Surg Oncol. 2011; 103: 435-41.
5. Minig L, Patrono MG, Romero N, Rodriguez Moreno JF, Garcia-Donas J. Different strategies of treatment for uterine cervical carcinoma stage IB2-IIB. World J Clin Oncol. 2014; 5: 86-92.
6. Ouderkirk JL, Krendel M. Non-muscle myosins in tumor progression, cancer cell invasion, and metastasis. Cytoskeleton (Hoboken). 2014; 71: 447-63.
7. Li YR, Yang WX. Myosins as fundamental components during tumorigenesis: diverse and indispensable. Oncotarget. 2016; 7: 46785-812.
8. Ma X, Adelstein RS. The role of vertebrate nonmuscle Myosin II in development and human disease. Bioarchitecture. 2014; 4: 88-102.
9. Bond LM, Tumbarello DA, Kendrick-Jones J, Buss F. Small-molecule inhibitors of myosin proteins. Future Med Chem. 2013; 5: 41-52.
10. Vicente-Manzanares M, Ma X, Adelstein RS, Horwitz AR. Non-muscle myosin II takes centre stage in cell adhesion and migration. Nat Rev Mol Cell Biol. 2009; 10: 778-90.
11. Higashi-Fujime S, Nakamura A. Cell and molecular biology of the fastest myosins. Int Rev Cell Mol Biol. 2009; 276: 301-47.
12. Medjkane S, Perez-Sanchez C, Gaggioli C, Sahai E, Treisman R. Myocardin-related transcription factors and SRF are required for cytoskeletal dynamics and experimental metastasis. Nat Cell Biol. 2009; 11: 257-68.
13. Li Q, Sarna SK. Nuclear myosin II regulates the assembly of preinitiation complex for ICAM-1 gene transcription. Gastroenterology. 2009; 137: 1051-60, 60 e1-3.
14. Zhang YS, Liu B, Luo XJ, Li TB, Zhang JJ, Peng JJ, et al. Nuclear cardiac myosin light chain 2 modulates NADPH oxidase 2 expression in myocardium: a novel function beyond muscle contraction. Basic Res Cardiol. 2015; 110: 38.
15. Huang L, Zheng M, Zhou QM, Zhang MY, Yu YH, Yun JP, et al. Identification of a 7-gene signature that predicts relapse and survival for early stage patients with cervical carcinoma. Med Oncol. 2012; 29: 2911-8.
16. Rankin EB, Giaccia AJ. Hypoxic control of metastasis. Science. 2016; 352: 175-80.
17. Wenger RH, Stiehl DP, Camenisch G. Integration of oxygen signaling at the consensus HRE. Sci STKE. 2005; 2005: re12.
18. Lu X, Kang Y. Hypoxia and hypoxia-inducible factors: master regulators of metastasis. Clin Cancer Res. 2010; 16: 5928-35.
19. Tewari KS, Sill MW, Long HJ, 3rd, Penson RT, Huang H, Ramondetta LM, et al. Improved survival with bevacizumab in advanced cervical cancer. N Engl J Med. 2014; 370: 734-43.
20. Penson RT, Huang HQ, Wenzel LB, Monk BJ, Stockman S, Long HJ, 3rd, et al. Bevacizumab for advanced cervical cancer: patient-reported outcomes of a randomised, phase 3 trial (NRG Oncology-Gynecologic Oncology Group protocol 240). Lancet Oncol. 2015; 16: 301-11.

21. Ebos JM, Lee CR, Cruz-Munoz W, Bjarnason GA, Christensen JG, Kerbel RS. Accelerated metastasis after short-term treatment with a potent inhibitor of tumor angiogenesis. Cancer Cell. 2009; 15: 232-9.

22. Paez-Ribes M, Allen E, Hudock J, Takeda T, Okuyama H, Vinals F, et al. Antiangiogenic therapy elicits malignant progression of tumors to increased local invasion and distant metastasis. Cancer Cell. 2009; 15: 220-31.

23. Lo Dico A, Costa V, Martelli C, Diceglie C, Rajata F, Rizzo A, et al. MiR675-5p Acts on HIF-1alpha to Sustain Hypoxic Responses: A New Therapeutic Strategy for Glioma. Theranostics. 2016; 6: 1105-18.

24. Balamurugan K. HIF-1 at the crossroads of hypoxia, inflammation, and cancer. Int J Cancer. 2016; 138: 1058-66.

25. de Lanerolle P, Serebryannyy L. Nuclear actin and myosins: life without filaments. Nat Cell Biol. 2011; 13: 1282-8.

26. de Lanerolle P. Nuclear actin and myosins at a glance. J Cell Sci. 2012; 125: 4945-9.

27. Bertout JA, Patel SA, Simon MC. The impact of O2 availability on human cancer. Nat Rev Cancer. 2008; 8: 967-75.

28. Vaupel P, Mayer A. Hypoxia in cancer: significance and impact on clinical outcome. Cancer Metastasis Rev. 2007; 26: 225-39.

29. Carmeliet P, Jain RK. Molecular mechanisms and clinical applications of angiogenesis. Nature. 2011; 473: 298-307.

30. Semenza GL. Hypoxia-inducible factors in physiology and medicine. Cell. 2012; 148: 399-408.

31. Wilson WR, Hay MP. Targeting hypoxia in cancer therapy. Nat Rev Cancer. 2011; 11: 393-410.

32. Ray M, Tang R, Jiang Z, Rotello VM. Quantitative tracking of protein trafficking to the nucleus using cytosolic protein delivery by nanoparticle-stabilized nanocapsules. Bioconjug Chem. 2015; 26: 1004-7.

33. Zhang L, Wang JH, Liang RX, Huang ST, Xu J, Yuan LJ, et al. RASSF8 downregulation promotes lymphangiogenesis and metastasis in esophageal squamous cell carcinoma. Oncotarget. 2015; 6: 34510-24.